Regeneration of frequency response functions from poles and zeros: a discussion with implications for cepstrum-based operational modal analysis

Wade A. SMITH[1]; Robert B. RANDALL[2]

[1,2] University of New South Wales, Australia

ABSTRACT

Operational modal analysis (OMA) seeks to determine a structure's dynamic characteristics from response-only measurements, which comprise both excitation and transmission path effects. The cepstrum has been used successfully in a number of applications to separate these source and path effects, after which the poles and zeros of the transfer function can be obtained via a curve-fitting process. The contributions from the individual poles and zeros can then be added (in log magnitude) to regenerate the frequency response function (FRF). This paper discusses a number of observations relating to this FRF regeneration process, as well as a number of broader points explaining FRFs from a pole-zero perspective. Among the topics covered in the discussion are: the required distribution of poles and zeros for the successful regeneration of FRFs; node points and weak modes in a pole-zero model; the differences in pole-zero distribution between receptance, mobility and inertance FRF forms; and, how to deal with the very low frequency region when regenerating FRFs. It is hoped that the discussion will assist in the application of cepstrum-based OMA methods and will lead to improved understanding of the FRF regeneration process and of frequency response functions more broadly.

Keywords: Modal analysis, Vibrating surfaces and structures, I-INCE Classification of Subjects Number(s): 75.6
(See http://www.inceusa.org/links/Subj%20Class%20-%20Formatted.pdf)

1. INTRODUCTION

Cepstrum-based operational modal analysis (OMA) was developed in the 1990s (1-5), and has recently received further attention (6-8). OMA seeks to determine the dynamic characteristics of a structure from response-only measurements, which comprise excitation and transmission path effects, which must be separated to obtain the latter. In certain cases, mostly involving a single input, the cepstrum can be used to conduct the separation, provided the two effects dominate distinct regions of the cepstrum. This relaxes the common assumption in OMA techniques that the input must be frequentially white.

Once the separation is complete, the frequency response functions (FRFs) of the system can be regenerated using the poles and zeros (resonances and anti-resonances) identified by curve-fitting the cepstrum of the corresponding transmission path. Through this process, the system is implicitly described using a pole-zero model, as opposed to the more common pole-residue model, the two being identical only for 'complete' models including all poles and zeros. Yet in practice there will almost inevitably be some truncation, in which only poles and zeros in a limited frequency band are used to describe the system as a whole. The FRFs regenerated from such a model have correctly located poles and zeros in the considered frequency band, but are subject to the effects of out-of-band poles and zeros, which manifest as a distortion of the general slope of the regenerated FRFs.

A number of techniques have been proposed to correct for this magnitude distortion, as outlined in Section 2.4 and addressed by the authors in (7). Through this process of refining techniques to regenerate FRFs from poles and zeros, the authors have identified a number of issues that warrant

[1] wade.smith@unsw.edu.au
[2] b.randall@unsw.edu.au

further discussion and explanation, and this is the basis of the present paper. It is hoped the discussion will assist in the application of cepstrum-based OMA methods and will lead to improved understanding of the FRF regeneration process.

2. BACKGROUND ON CEPSTRUM-BASED OMA

2.1 The cepstrum defined

Various definitions for the cepstrum exist (9); here we shall use the so-called 'real cepstrum' $\hat{x}$ and 'complex cepstrum' $\hat{x}_c$, defined for some time signal $x(t)$ as:

$$\hat{x}(\tau) = \Im^{-1}\left[\log\left(\left|X(f)\right|\right)\right] \quad \text{and} \quad \hat{x}_c(\tau) = \Im^{-1}\left[\log\left(X(f)\right)\right] \tag{1}$$

where $X(f) = \Im[x(t)]$ is the (complex-valued) Fourier transform of $x(t)$. Table 1 includes a number of terms often employed when using the cepstrum. Note that the real cepstrum includes no phase information, so the original time signal is not recoverable after liftering in the cepstrum domain. However, the process from the amplitude spectrum to the real cepstrum is reversible, and so the amplitude spectrum can be obtained after cepstral editing (10), as exploited in this paper. The 'complex' cepstrum is also real-valued, but includes phase information from the spectrum so is fully invertible; thus, $x(t)$ can be recovered after liftering the cepstrum.

Table 1 – Cepstrum terminology

Frequency domain	Cepstrum domain
Frequency	Quefrency
Spectrum	Cepstrum
Filtering	Liftering
Low-pass filter	Short-pass lifter
High-pass filter	Long-pass lifter

2.2 Separation of source and path effects

While OMA possesses a number of advantages over EMA (where excitation forces are measured), its reliance on response-only measurements requires different techniques in order to extract modal properties. Response measurements, of course, typically comprise both excitation and transmission path effects, and these need to be separated before the structural properties can be determined.

For a linear time-invariant (LTI) system subjected to a single input $x(t)$, the system response $y(t)$ is the convolution of the input and the impulse response function $h(t)$:

$$y(t) = h(t) * x(t) = \int_{-\infty}^{\infty} h(\tau) \cdot x(t-\tau) \cdot d\tau \tag{2}$$

In the frequency domain, expressing the relationship in terms of the complex spectra (or Fourier transforms of the time records), the convolution becomes multiplicative:

$$Y(f) = H(f) \cdot X(f) \tag{3}$$

in which $H(f)$ is the frequency response function (FRF). For the real cepstrum the respective moduli can be used. Taking the log and the inverse Fourier transform, we obtain the cepstra, in which source and path effects are additive:

$$\hat{y}(\tau) = \hat{h}(\tau) + \hat{x}(\tau) \quad \text{and} \quad \hat{y}_c(\tau) = \hat{h}_c(\tau) + \hat{x}_c(\tau) \tag{4}$$

Thus in circumstances in which the input occupies defined regions of the cepstrum, the source effects can easily be separated (via appropriate liftering) from those of the transmission path, which usually occupy a broader quefrency range. Examples of such inputs include frequentially smooth and flat forces, which are concentrated in the low quefrency region, such as a hammer blow, which does not have to be white (4). Such an input can be removed from the response cepstrum via long-pass liftering, leaving only the path cepstrum, from which the system's FRF can be recovered. It should be noted that this is a much less restrictive requirement than the common white noise input assumption made by most other OMA techniques.

2.3 Representation of transmission path effects

Employing a pole-zero (as opposed to pole-residue) model, the transfer function (from which the FRF is obtained by evaluating along the imaginary axis) can be represented as:

$$H(s) = \frac{B\prod_{n=1}^{N_z}(s-z_n)(s-z_n^*)}{\prod_{k=1}^{N_p}(s-p_k)(s-p_k^*)} \tag{5}$$

where N_p is the number of modal frequencies (or poles) considered in the model, p_k are the system's (complex) poles, N_z is the number of (complex) zeros (anti-resonances), z_n, considered in the model, and B is a scaling factor. As can be seen, the poles and zeros occur in complex conjugate pairs, although in some cases there are also real poles and zeros, as discussed in later sections.

Any real structure will have an infinite number of modes, and so by limiting N_p (and N_z) to a finite value (by restricting the frequency range of interest, say), the model becomes a truncated representation of the complete system. The numerator and denominator in Eq. (5) can be visualised as being the product of distances from a given point in the *s*-plane to the zeros and poles, respectively. Thus poles and zeros outside the frequency band of interest manifest as a distortion of the magnitude of $H(s)$ in a frequency-dependent manner; the in-band poles and zeros will be represented accurately, but the residues will be distorted. Transfer functions with a greater imbalance between numbers of poles and zeros will be more susceptible to this magnitude distortion. In the context of a chain-like structure, such as a beam, the greater the distance between source and response, the greater the imbalance between the numbers of poles and zeros (5).

For a sampled sequence, the transfer function of Eq. (5) can be expressed in the z-plane as:

$$H(z) = \frac{Bz^r\prod_{k=1}^{N_{zi}}(1-a_k z^{-1})\prod_{k=1}^{N_{zo}}(1-b_k z)}{\prod_{k=1}^{N_{pi}}(1-c_k z^{-1})\prod_{k=1}^{N_{po}}(1-d_k z)} \tag{6}$$

where a_k and c_k represent the zeros and poles inside the unit circle, and $1/b_k$ and $1/d_k$ the zeros and poles outside the unit circle, respectively (where $|a_k|,|b_k|,|c_k|,|d_k| < 1$).

Based on a more general expression by Oppenheim and Schafer (11), Gao and Randall (2) showed that for a stable minimum phase system (applies to many simple mechanical systems), the complex cepstrum corresponding to $H(z)$ can be expressed in terms of the zeros and poles inside the unit circle:

$$\hat{h}_c(n) = \begin{cases} \log|B| & n = 0 \\ 2\sum_{k=1}^{N_{pi}/2}\frac{A_{ck}^n}{n}\cos(\omega_{ck}n) - 2\sum_{k=1}^{N_{zi}/2}\frac{A_{ak}^n}{n}\cos(\omega_{ak}n) & n > 0 \\ 0 & n < 0 \end{cases} \tag{7}$$

in which n is the quefrency index and where, for example, a pair of poles, c_k, has been replaced by $(2/n)A_{ck}^n\cos(\omega_{ck}n)$, in which $A_{ck} = |c_k|$ and $\omega_{ck} = \angle c_k$ represent, for each pole, the damping and the damped natural frequency, respectively, and likewise for the zeros a_k. (Implicit in the above is that the Fourier transforms of Eq. (1) have been replaced by z-transforms in the calculation of the cepstrum.)

Thus, according to Eq. (7), by curve-fitting a liftered form of the response cepstrum (to remove source effects), one can obtain the transfer function's poles and zeros. From these poles and zeros, the FRF can be regenerated to within a scaling factor, since B is not recovered from the curve-fitting process. However, the obtained FRF will still be subject to the previously-mentioned distortion associated with truncation. In general, therefore, to obtain the system's true FRFs, the FRF regeneration process needs to account for both overall and relative scaling factors.

2.4 Magnitude equalisation of regenerated FRFs

A number of techniques have been proposed to generate a magnitude equalisation curve to correct for the effects of truncation, including the 'phantom zero' approach of Randall *et al.* (5). Hanson *et al.* (12, 13) applied cepstrum OMA to certain multiple-input-multiple-output (MIMO) applications. Their technique to determine the magnitude equalisation curve was to compare the OMA-regenerated FRF with one obtained from an updated finite element model. The poles and zeros found via the OMA

process were used to update the FE model, from which an FRF was determined and compared with the OMA-regenerated FRF. The (log magnitude) difference between the two FRFs was then used to develop the equalisation curve, which was in turn used to correct the distorted slope of the OMA-regenerated FRF.

One difficulty that arises in basing the magnitude equalisation curve on the difference between two FRFs is that any misalignment of the poles and zeros in the FRFs results in a series of peak/notches that need to be smoothed or filtered out. Hanson *et al*. (12, 13) achieved this by transforming the difference curve into the cepstrum domain, short-pass liftered the resulting cepstrum – since the peak/notches would typically occupy the higher quefrency region – and then transforming back to the frequency domain. The resulting equalisation curve, however, had a noticeable 'ripple' throughout the frequency range, presumably caused by end effects during the Fourier transform(s).

The present authors proposed a simple alternative approach to obtain a smoothed equalisation curve, based on polynomial curve fitting of the (log magnitude) difference between the regenerated and reference FRFs (7). The reference FRF could be found by a finite element model, as used by Hanson *et al.*, or simply the FRF measured through conventional experimental modal analysis (EMA) techniques, but not under operational conditions.

The method has a number of advantages over the aforementioned phantom zeros and cepstral filtering approaches. When executed with a basic constrained optimisation algorithm, for example, it allows the user to specify a particular point, or points, through which the scaled FRF curve must pass. This would be especially useful for the correct scaling of the very low frequency (VLF) region of the FRF, which was not executed well with the liftering approach (7). This is particularly important because the behaviour of structures in the VLF region is usually well understood theoretically but is often masked in EMA-based measurements.

Fig. 1 shows the proposed OMA process summary as outlined by the authors in (7).

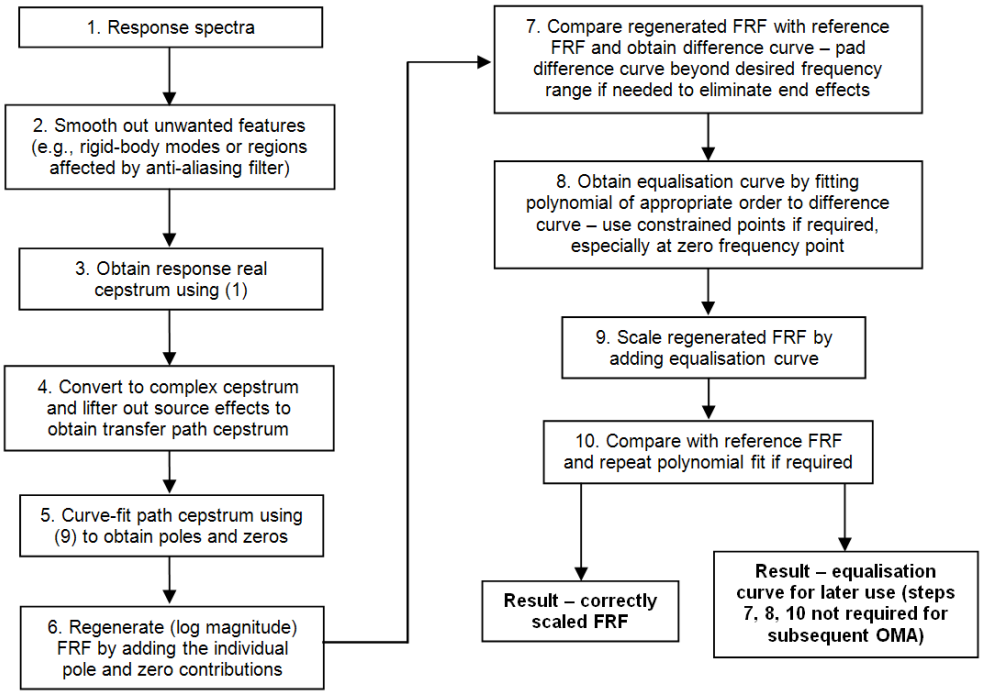

Figure 1 – Summary of proposed OMA process (7)

3. INITIAL EXPERIMENTAL RESULTS

3.1 Experimental setup

The technique outlined in the previous sections was applied to a steel beam test rig, as outlined in (13) and shown in Fig. 2. The beam (20 x 50 x 1000 mm) was supported on soft springs to represent free-free boundary conditions, with the highest rigid-body mode at 5 Hz well separated from the first bending mode of 95 Hz.

The beam was excited with a frequentially smooth input through a shaker mounted at one end of the

beam (point 1 in Fig. 2) and on its longitudinal centreline. This ensured for simplicity that only the bending modes were excited. The excitation was burst random noise with a cycle of 250ms on / 250ms off. The noise, with frequency content ranging from 0–2048 Hz, was subjected to coloured filtering to approximate pink noise. This was done to introduce distortion of the response spectra – an intentional violation of the typical OMA 'white noise' assumption – while maintaining a 'frequentially smooth' input, to allow for cepstrum-based source-path separation. Such distortion means that both the overall and relative scaling of each mode is lost in the response spectra.

The acceleration response was measured at 11 equi-spaced points along the longitudinal centreline of the beam, as shown in Fig. 2. Each response was measured for a duration of ten minutes and was sampled at 4096 Hz. The long measurement record allowed for sufficient averaging to obtain for each response a smooth spectral density. The applied force was also measured to allow for the determination of reference FRFs through conventional EMA techniques.

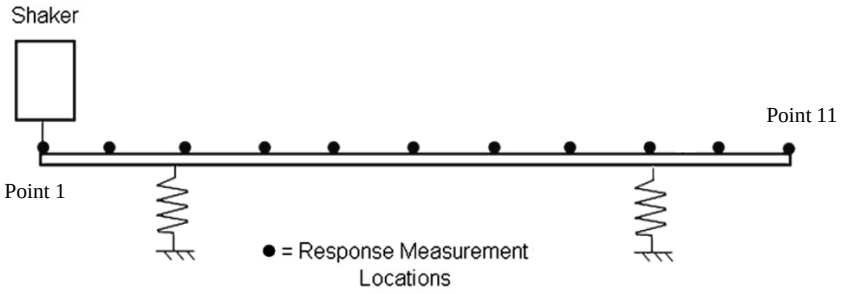

Figure 2 – Representation of steel beam test setup (adapted from (12))

3.2 Results and discussion

Shown in Fig. 3 (top) are the frequency response functions (expressed as accelerance) regenerated using the cepstrum OMA approach before carrying out any scaling. These were first reported by the authors in (7). Included in the plots for comparison are the FRFs obtained through conventional EMA techniques. The FRFs relate to points 1 (driving point) and 11, which were chosen to represent the two extremes, one having (nearly) equally balanced poles and zeros, and the other having only poles. The effect of this (im)balance between numbers of poles and zeros is clearly seen in the general slope of the regenerated FRFs as compared with their measured counterparts, with the regenerated FRF of point 11 exhibiting significant distortion (up to 40 dB difference from the EMA value).

Note that the poles and zeros above about 1600 Hz are not represented in the regenerated FRFs because they were filtered out prior to conducting the cepstrum curve-fitting (based on Eq. (7)). Also filtered from the response spectra prior to the cepstrum curve-fitting were the low-frequency rigid-body modes of the beam oscillating on the soft spring supports, which were not of interest in this study and could have distorted the response cepstra.

Shown in Fig. 3 (bottom) are the scaled versions of the regenerated FRFs, again plotted alongside the EMA results. The regenerated FRFs have been scaled by the polynomial-based equalisation curve, as outlined previously. It can be seen that now the regenerated and measured FRFs are almost indistinguishable from one another.

Fig. 4 shows the equalisation curves used to scale the regenerated FRFs from Fig. 3. Also plotted are the log magnitude difference curves between the measured and regenerated FRFs, in which the series of peak notches is clearly seen. To obtain the equalisation curves, polynomials were fitted to the difference curves with the only constraint being that the curves pass through the theoretical zero-frequency accelerance value (shown as a small dot in Fig. 4). This process was implemented as a constrained linear least-squares optimisation problem using MATLAB's in-built 'lsqlin' function.

Although this equalisation process ultimately produced very good results, the authors were concerned about the FRF behaviour in the VLF region. In particular, it was thought that outside the frequency range containing poles and zeros, the equalisation curve should be monotonic, as from observation it seems that the effects of (high frequency) out-of-band modes have a monotonic nature. Yet the equalisation curve for the transfer point in Fig. 4 is far from monotonic, requiring a tenth order polynomial to properly represent the abrupt change in curvature in the VLF region. This prompted an investigation of FRF behaviour in this frequency range.

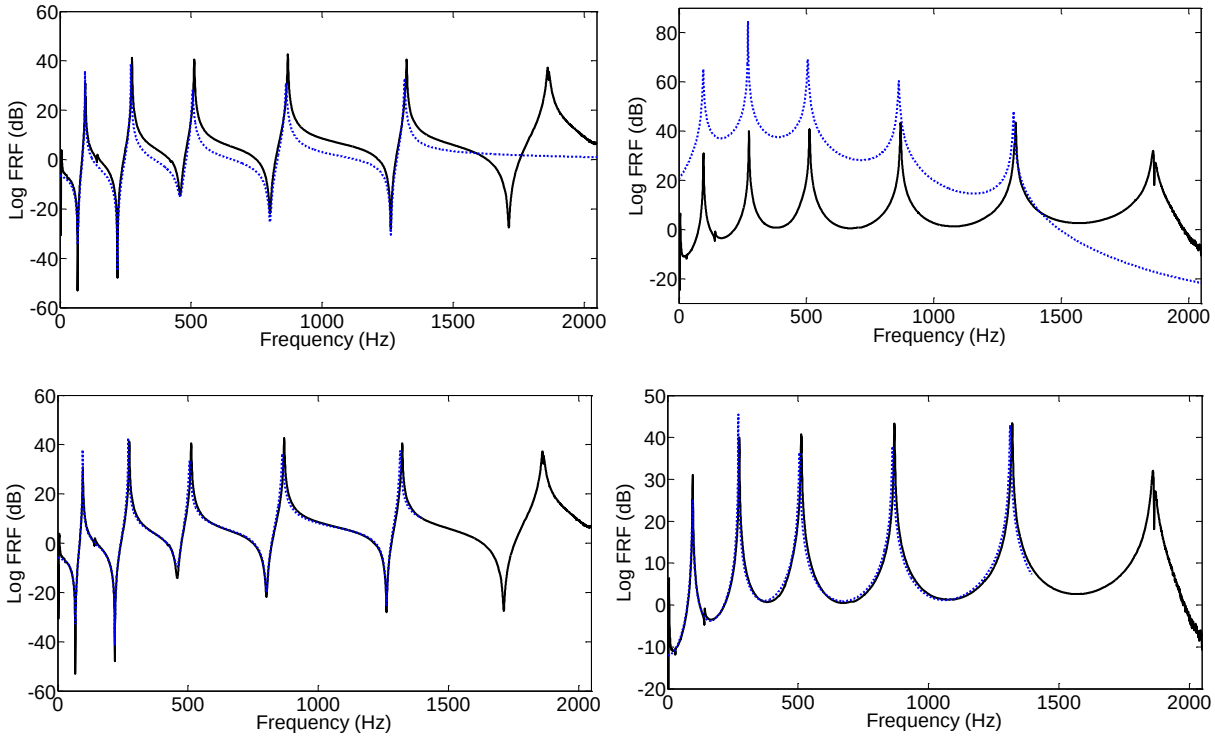

Figure 3 – Drive point (left) and transfer (right) FRF comparison. Top: effect of truncation: measured (—), regenerated from OMA without scaling (⋯). Bottom: effect of polynomial-based equalisation curve: measured (—), regenerated from OMA and scaled (⋯) (7)

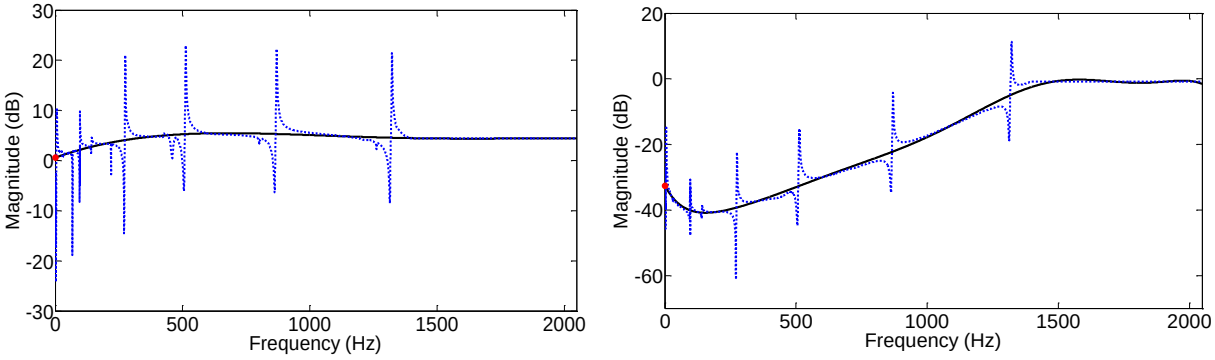

Figure 4 – Drive point (left) and transfer (right) equalisation curves obtained from polynomial curve-fitting, as used in Figure 3: equalisation curves (—), raw difference curves between measured and OMA-regenerated FRFs showing series of peak/notches (⋯) (7)

4. INVESTIGATING FRF BEHAVIOUR IN THE VERY LOW FREQUENCY REGION

4.1 Fixed boundary system

To investigate the behavior of the regenerated FRFs in the VLF region, a simple undamped 2DOF model was established, as shown in Fig. 5.

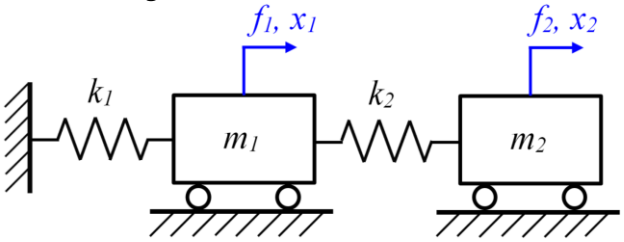

Figure 5 – Undamped 2DOF model

Assuming steady state conditions, we can express the output of the system as a function of the excitation force and FRF terms:

$$\mathbf{X}(\omega) = \mathbf{H}_r(\omega)\mathbf{F}(\omega) \tag{8}$$

in which $\mathbf{X} = \{X_1, X_2\}^T$ and $\mathbf{F} = \{F_1, F_2\}^T$, and $\mathbf{H}_r$ is the *receptance* FRF matrix, which can be easily obtained as:

$$\mathbf{H}_r(\omega) = \frac{1}{a_2\omega^4 - a_1\omega^2 + a_0}\begin{bmatrix} -m_2\omega^2 + k_2 & k_2 \\ k_2 & -m_1\omega^2 + k_{tot} \end{bmatrix} \tag{9}$$

in which $a_2 = m_1m_2$, $a_1 = m_1k_2 + m_2k_1 + m_2k_2$, $a_0 = k_1k_2$ and $k_{tot} = k_1 + k_2$. The roots of the denominator and numerator in Eq. (9) represent, for the given FRF, the poles and zeros, respectively.

This equation illustrates or conforms to a number of well-known points for the FRFs of chain-like structures: that there generally exists (almost) as many zeros as poles in driving point FRFs (H_{11} and H_{22}) but as the distance between the input-output points increases the number of zeros decreases, until at the extreme transfer case there are no zeros (H_{12} and H_{21}). This can be physically understood as extreme transfer points alternating in relative phase relationships in successive resonances, while driving points maintain the same phase relationships in successive resonances and thus require a zero between each pair of poles to 'reverse' the phase jump from the last resonance.

Another feature of Eq. (9) is that in general there will be no DC (zero frequency) poles or zeros, but non-DC poles and zeros will occur symmetrically about the zero-frequency axis. (In the general case involving damping, it is well-known that the poles and zeros will either be purely real or appear in complex conjugate pairs; this is assumed but not proven here.)

This form of the FRF represents the receptance case, but mobility $(\dot{X}/F)$ and especially accelerance $(\ddot{X}/F)$ are often used, in which case we need to multiply $\mathbf{H}_r$ by $j\omega$ and $(j\omega)^2$, respectively, to give the correct FRF form:

$$\mathbf{H}_m(\omega) = j\omega\mathbf{H}_r(\omega) \quad \text{and} \quad \mathbf{H}_a(\omega) = -\omega^2\mathbf{H}_r(\omega) \tag{10}$$

In bringing extra ω terms into the numerator, DC zeros are created – one in the mobility case and two in the accelerance case.

4.2 Free boundary system

Now let us take the free support case, which is the one most often used in laboratory modal testing. Setting $k_1 = 0$ in Fig. 5, the receptance FRFs matrix becomes:

$$\mathbf{H}_r(\omega) = \frac{1}{\omega^2\left(a_2\omega^2 - \bar{a}_1\right)}\begin{bmatrix} -m_2\omega^2 + k_2 & k_2 \\ k_2 & -m_1\omega^2 + k_2 \end{bmatrix} \tag{11}$$

in which $\bar{a}_1 = k_2\left(m_1 + m_2\right)$ and the constant term (a_0) in the denominator of Eq. (9) vanishes to create two DC poles, which is not surprising since with any free boundary structure we should expect rigid body modes. Following the same conversion to mobility and accelerance as in Eq. (10) again yields one DC zero in the mobility case and two in the accelerance case.

4.3 DC poles and zeros summarised

These DC pole-zero characteristics are summarized in Table 2. It can be seen that the only cases for which the DC poles and zeros balance are the fixed boundary receptance FRF and the free boundary accelerance FRF.

Table 2 – DC pole-zero characteristics

FRF form	Fixed boundary	Free boundary
Receptance	no pole, no zero	two poles, no zero
Mobility	no pole, one zero	two poles, one zero
Accelerance	no pole, two zeros	two poles, two zeros

Now we can relate these DC pole-zero characteristics back to the well-known classical (log-log) FRF forms, as given for example in (14, 15) and shown in Fig. 6 for our 2DOF model. It can be seen that the FRF is asymptotic to lines of constant mass or stiffness (straight lines on a log-log scale) in the VLF and very high frequency (VHF) regions, and in particular we note that the asymptotic slope of a given FRF in the VLF region is determined by the balance of DC poles and zeros, taking an integer value (on a log-log scale) from –2 in the free boundary receptance case (two poles, no zero) to +2 in the fixed boundary accelerance case (no pole, two zeros). Perhaps a more familiar representation of these gradients is in terms of decibels (shown in the figures), where a slope of 1 is 20 dB/decade – unsurprisingly, the roll-off gradient for a first order filter.

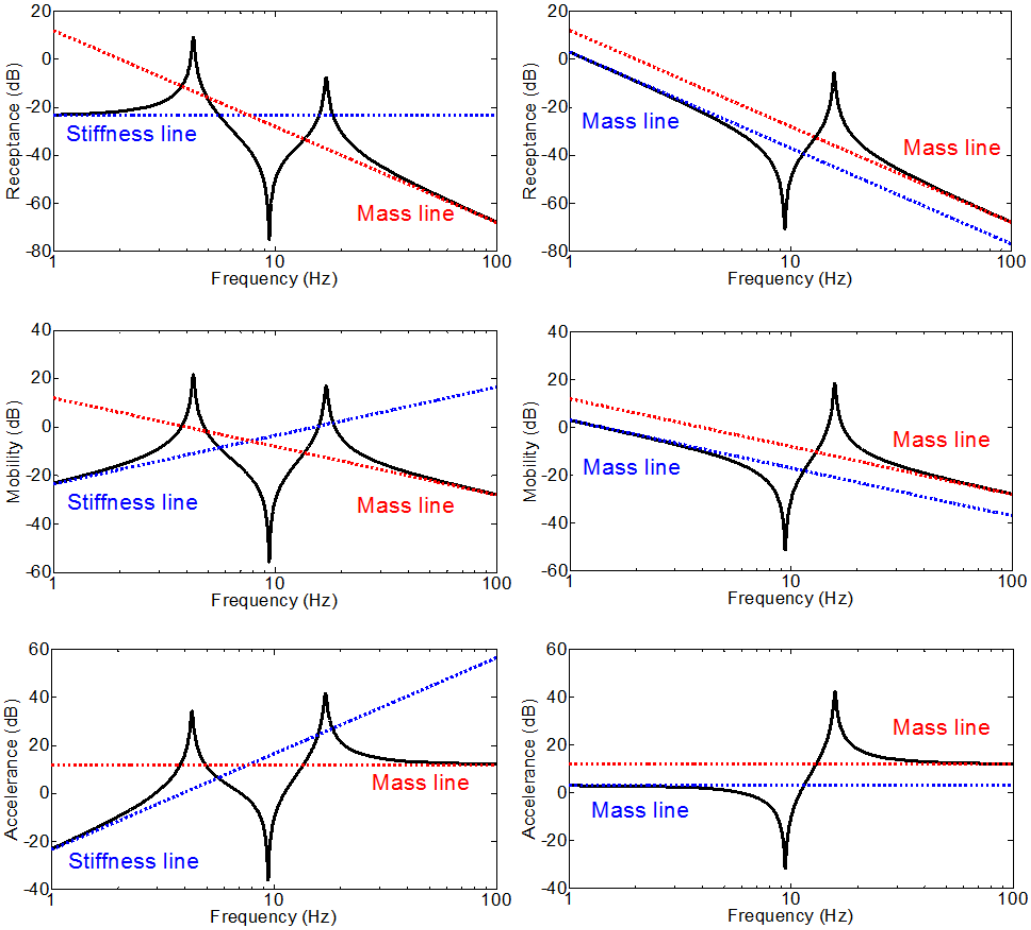

Figure 6 – Drive point frequency response functions for fixed (left) and free (right) boundary conditions: receptance (top), mobility (middle) and accelerance (bottom); corresponding mass and stiffness lines representing asymptotic VLF (···) and VHF (···) characteristics

Yet despite this explanation for the behaviour of FRFs in the VLF region, it does not explain the VLF zero-gradient characteristics of the balanced DC pole-zero cases (fixed boundary receptance and free boundary accelerance), which of course is what prompted the initial investigation.

4.4 New results including negative frequency poles and zeros

It has since been realised that to achieve these characteristics with a pole-zero model, the negative frequency poles and zeros (or, more generally, the complex conjugate pairs) must be included in the regeneration process. To neglect them is in fact to truncate the model unnecessarily, and although earlier papers (2, 12) had focused precisely on this point in regard to high frequency modes, the same truncation effect from the negative frequency region had not been appreciated. Indeed, this was so even in the present authors' recent work (7), as discussed previously and shown in Fig. 3, where the (unscaled) regenerated transfer FRF (top-right) does not follow the mass line in the VLF region, and consequently the corresponding equalisation curve (Fig. 4) requires an abrupt change in curvature to achieve a sufficient correction. In the context of a polynomial-based equalisation curve (7), this means a much higher order polynomial would be used than what was truly required.

Fig. 7 illustrates this point by using the same data as in Fig. 3, but now including the regenerated FRF (transfer case only) using both positive and negative frequency poles and zeros. It is seen here that the new FRF conforms to the expected VLF behaviour, flattening out to the mass line near zero frequency. Meanwhile, the corresponding FRF difference curve – on which the equalisation curve is based – now shows the basic monotonic trend that had initially been expected.

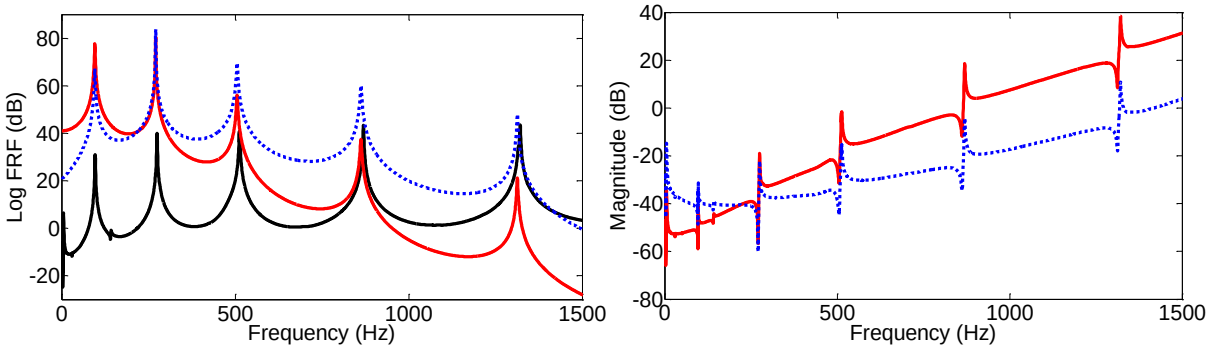

Figure 7 – Transfer FRFs (left) and corresponding raw difference curves between measured and OMA-regenerated FRFs (right): measured (—), regenerated from OMA without negative frequency poles and zeros (···), regenerated from OMA with negative frequency poles and zeros (—)

5. IMPLICATIONS FOR REGENERATING FRFS FROM POLES AND ZEROS

It is clear from the preceding section that a certain distribution of poles and zeros is required to give the best regeneration of FRFs. That section concentrated on FRF characteristics in the VLF region, where DC and negative frequency poles and zeros were shown to dictate VLF behaviour. But it is perhaps worth mentioning a couple of further points that will hopefully guide the analyst in the FRF regeneration process. A key point here is that all FRF information should be contained in the poles and zeros, except for an overall scaling factor and the effects of out-of-band modes, and so any FRF phenomenon should be describable in terms of its poles and zeros.

5.1 Weak modes and node points

One phenomenon that is perhaps not so clear from a pole-zero perspective is that of a weak mode. Unlike in a pole-residue model, where modal contributions are scaled explicitly, a pole-zero model relies on the scaling effect of neighbouring poles and zeros, the individual contributions of which are simply added (in log magnitude) to give the complete FRF. Thus it becomes clear that to represent a weak mode with a pole-zero model, the placement of a zero in close proximity to the pole would generally be required (this may not be so if the pole is in a region of relative modal sparsity).

Following on from weak modes, we must also be able to describe node points with a pole-zero model. Given that poles are global system properties, they do not simply disappear in the event of node points. Thus the only way to negate the effects of a pole is through cancellation with a zero, i.e. a zero must occur at exactly the same frequency as the pole to be negated. This was explained by Mottershead and Lallement (16), and although pole-zero cancellation is well-known in the control field, its use in describing vibration nodes does not seem to have been widely appreciated.

The weak pole and node point concepts can be easily linked, at least in chain-like structures, by considering a zero to 'pass by' a given pole, reducing the strength of the pole until the point of intersection, whereupon a node occurs.

5.2 Practical implications

The practical implications of the above points are particularly apparent when considering zeros. Unlike poles, the zeros in practical measurements are often buried in noise and are not always so clear. In the application of cepstrum OMA, this makes it difficult to choose how many zeros to use when establishing the pole-zero model. This issue was considered recently by Dackermann *et al.* (8), where different numbers of zeros were used to regenerate FRFs for structural health monitoring purposes. In such cases, a thorough understanding of expected pole-zero distributions can help the analyst to regenerate better FRFs. For example, the knowledge that in a pole-zero model, a weak mode can only be represented by placing a zero in close proximity allows the analyst to achieve such a feature.

6. CONCLUSIONS

This paper has discussed a number of issues surrounding the regeneration of frequency response functions from poles and zeros. This is particularly relevant to cepstrum-based operational modal analysis, which requires the use of a pole-zero model to represent the system. Emphasis is given to the behaviour of FRFs in the very low frequency region, and in particular to the specific distribution of poles and zeros required to regenerate FRFs correctly. It is pointed out that negative frequency poles and zeros should be included in the regeneration process, along with the correct balance of DC poles and zeros.

It is hoped the discussion will assist in the application of cepstrum-based OMA methods and will lead to improved understanding of the FRF regeneration process and of frequency response functions more broadly.

ACKNOWLEDGEMENTS

The authors would like to thank David Hanson for the use of his experimental data. This research was supported by the Australian Research Council and SpectraQuest, through Linkage Project [LP110200738].

REFERENCES

1. Gao Y, Randall RB, editors. Zeros Vs Residues. 17th International Seminar on Modal Analysis; 1992; K. U. Leuven, Belgium. Katholieke Universiteit Leuven.
2. Gao Y, Randall RB. Determination Of Frequency Response Functions From Response Measurements—I. Extraction Of Poles And Zeros From Response Cepstra. Mechanical Systems and Signal Processing. 1996;10(3):293-317.
3. Gao Y, Randall RB. Determination Of Frequency Response Functions From Response Measurements—II. Regeneration Of Frequency Response Functions From Poles And Zeros. Mechanical Systems and Signal Processing. 1996;10(3):319-40.
4. Randall RB, Gao Y. Extraction Of Modal Parameters From The Response Power Cepstrum. Journal of Sound and Vibration. 1994;176(2):179-93.
5. Randall RB, Gao Y, Sestieri A. Phantom zeros in curve-fitted frequency response functions. Mechanical Systems and Signal Processing. 1994;8(6):607-22.
6. Dackermann U, Smith WA, Randall RB. Damage identification based on response-only measurements using cepstrum analysis and artificial neural networks. Structural Health Monitoring. 2014;13(4):430-44.
7. Randall RB, Smith WA, Cepstrum-based operational modal analysis: regeneration of frequency response functions. Proceedings of 7th Australasian Congress on Applied Mechanics (ACAM 7); 2012 9-12 December; Adelaide, Australia.
8. Dackermann U, Smith WA, Li J, Randall RB. On the use of the cepstrum and artificial neural networks to identify structural mass changes from response-only measurements. ISMA; 15-17 September; Leuven, Belgium2014.
9. Childers DG, Skinner DP, Kemerait RC. The cepstrum: A guide to processing. Proceedings of the IEEE. 1977;65(10):1428-43.
10. Randall RB. Vibration-based Condition Monitoring: Industrial, Aerospace and Automotive Applications. West Sussex, United Kingdom: John Wiley & Sons, Ltd; 2011.
11. Oppenheim AV, Schafer RW. Discrete-Time Signal Processing. Third ed. Oppenheim AV, editor. Upper Saddle River, NJ: Pearson Higher Education; 2010.
12. Hanson D, Randall RB, Antoni J, Thompson DJ, Waters TP, Ford RAJ. Cyclostationarity and the cepstrum for operational modal analysis of MIMO systems—Part I: Modal parameter identification. Mechanical Systems and Signal Processing. 2007;21(6):2441-58.
13. Hanson D, Randall RB, Antoni J, Waters TP, Thompson DJ, Ford RAJ. Cyclostationarity and the cepstrum for operational modal analysis of MIMO systems—Part II: Obtaining scaled mode shapes through finite element model updating. Mechanical Systems and Signal Processing. 2007;21(6):2459-73.
14. Ewins DJ. Modal Testing: Theory, Practice and Application. Second ed. Baldock, England: Research Studies Press Ltd; 2000.
15. Salter JP. Steady-State Vibration. Hampshire, UK: Kenneth Mason; 1969. 166 p.
16. Mottershead JE, Lallement G. Vibration Nodes, and the Cancellation of Poles and Zeros by Unit-Rank Modifications to Structures. Journal of Sound and Vibration. 1999;222(5):833-51.